

Conceptual Design of a BLI Propulsor Capturing Aero-Propulsive Coupling and Distortion Impacts

Manish Pokhrel*, Mingxuan Shi*, Jai Ahuja*, Jonathan Gladin[†]
and Dimitri N. Mavris[‡]

*Aerospace Systems Design Laboratory, School of Aerospace Engineering,
Georgia Institute of Technology, Atlanta, Georgia, 30332*

Boundary Layer Ingestion (BLI) appears to be a promising solution to meet aggressive aviation fuel burn and environmental goals defined by NASA and other entities. Propulsion-airframe integration plays a critical role in BLI vehicle design given the strong coupling between the airframe and the propulsion system. Several studies have focused on flow field impacts on the propulsion system performance, but have ignored the effect of the propulsor on the flow field. Recent studies, however, have focused on both aspects, highlighting the need for capturing this interdisciplinary coupling. Multidisciplinary analyses (MDA), especially those involving CFD, are computationally expensive and are not suitable in the conceptual design of BLI propulsion systems. This paper aims to provide a less expensive approach by developing a parametric formulation for the effect of the propulsion system on the flow field, which can then be used in BLI propulsor conceptual design. This paper quantifies the sensitivity of the changes in the flow field due to the on-design and off-design parameters of the propulsion system. In addition, it also illustrates the difference in propulsion system design and performance when the throttle dependent effects on the flow field is captured, to the case where it is not. Distortion impacts on engine sizing and performance are also considered in this paper.

I. Nomenclature

A	Area	<i>Subscripts</i>	
D'	Total aircraft drag (without BLI engine)	base	Reference/baseline configuration
$dPcP$	Distortion intensity	clean	Isolated airframe (no engine)
F_N	Net momentum flux through propulsor	crit	Critical angle
F_X	Net streamwise force on an aircraft	e , out	Propulsor exit
\dot{m}	Mass flow rate	ed	Boundary layer edge
M	Mach number	in	Propulsor inlet
$\hat{\mathbf{n}}$	Unit normal for boundary surface	j , jet	Jet exhaust
p	Static pressure	surf	Airframe surface
P_K	Net propulsive mechanical power	t	Stagnation quantity
V	Velocity magnitude	tot	Total value for airframe
\mathbf{V}	Velocity vector	vortex	Trailing vortex sheet
η_{PR}	Pressure recovery (p_{t_2}/p_{t_0})	wake	Aircraft wake
κ	Kinetic energy defect	0	Engine station: Ambient
ρ	Density	1	Engine station: Inlet highlight plane
Φ	Dissipation rate	2	Engine station: Fan face
ζ	BLI Effect $\equiv P_{K_{in}} + \Delta\Phi_{wake}$		

*PhD Candidate, Aerospace Systems Design Laboratory, Georgia Institute of Technology, AIAA Student Member

[†]Research Engineer II, Aerospace Systems Design Laboratory, Georgia Institute of Technology, AIAA Member

[‡]S.P. Langley Distinguished Regents Professor, Georgia Institute of Technology, AIAA Fellow

II. Introduction

Tube and wing configurations with podded engines have been predominant in the commercial aviation industry for decades. However, stringent aviation goals such as the N+3 targets put forth by NASA¹ necessitate configuration changes for the current aircraft fleet. As a consequence, newer concepts with tightly integrated airframe and propulsion systems with other enabling technologies have emerged, as part of ongoing research. Boundary Layer Ingestion (BLI) is one such option that aims to reduce vehicle fuel burn.

A. BLI and Fuel Burn Benefits

The idea of BLI for aircraft was proposed by Smith in the 1940s.² While subsequent research focused on BLI for marine applications,^{3,4} research interest in BLI for commercial transport aircraft, as a means for improving fuel efficiency, has grown rapidly in the last two decades. Liu⁵ summarized the system level benefits of BLI reported in several studies, noting 3-10% fuel burn savings depending on the type of configuration studied. Simple equations involving propulsive power and thrust can demonstrate fuel burn savings from BLI. The net momentum flux for an isolated engine (or net thrust), ingesting freestream flow, is given by Eq. (1). The power provided by the engine to produce this thrust is equal to the difference in the kinetic energy rate of the flow exiting and entering the propulsor, and is proportional to the net momentum flux as seen in Eq. (2). Eqns. (3) and (4) show the net momentum flux and propulsive power requirements for the BLI case.

$$F_N = \dot{m}(V_j - V_\infty) \quad (1)$$

$$P = \frac{\dot{m}}{2}(V_j^2 - V_\infty^2) = \frac{F_N}{2}(V_j + V_\infty) \quad (2)$$

$$F_{N_{BLI}} = \dot{m}_{BLI}(V_{j_{BLI}} - V_{BLI}) \quad (3)$$

$$P_{BLI} = \frac{\dot{m}_{BLI}}{2}(V_{j_{BLI}}^2 - V_{BLI}^2) = \frac{F_{N_{BLI}}}{2}(V_{j_{BLI}} + V_{BLI}) \quad (4)$$

In the BLI case, to produce the same net momentum flux across the propulsor ($F_{N_{BLI}} = F_N$) given the lower inlet velocity ($V_{BLI} < V_\infty$), and assuming the BLI propulsor is sized to ingest the same mass flow rate as the non-BLI engine ($\dot{m}_{BLI} = \dot{m}$), the jet velocity for the BLI case must be lower than that for the non-BLI case ($V_{j_{BLI}} < V_j$). This implies a lower gross thrust requirement since the ram drag decreases. This also implies a lower propulsive power requirement for the same net momentum flux across the propulsor, since $V_{j_{BLI}} + V_{BLI} < V_j + V_\infty$, which results in a reduction in fuel burn.

B. BLI Modeling

The idea of bookkeeping aircraft performance in terms of thrust and drag is a common practice for conventional tube and wing vehicles with podded engines. However for BLI systems, the distinction between thrust and drag becomes unclear. The airframe boundary layer flow ingested by the propulsors contributes to both thrust and drag and separating these contributions is difficult.⁶ To shy away from this confusion, one can use the power balance bookkeeping approach proposed by Drela⁷ to analyze BLI systems. Regardless of the bookkeeping approach used, the flow on the airframe affects propulsor sizing and performance, which in turn affects the ingested airflow as shown by Gray.⁸ Both these interactions need to be captured in the modeling process. The power balance bookkeeping approach for a BLI vehicle can be formulated as shown in Eq.(5).⁶

$$P_K - \Phi_{jet} = \Phi_{surf} + \Phi_{wake} + \Phi_{vortex} - F_X V_\infty \quad (5)$$

P_K represents the net propulsive mechanical power into the control volume, and has non-zero contributions only at the propulsor inlet and exit planes. Thus, P_K can be expressed as:

$$P_K = P_{K_{in}} + P_{K_{out}} \quad (6)$$

Φ_{jet} represents the jet mixing dissipation from the propulsor exhaust. The Φ terms on the right hand side of Eq. (5) represent dissipation contributions from several sources: airframe surface, wake, and in the trailing

vortex sheet. $F_X V_\infty$ represents the excess power requirement for the aircraft, which is zero at the cruise condition. Rearranging Eq. (5) and using Eq. (6), while assuming cruise conditions, one can obtain:

$$P_{K_{out}} - \Phi_{jet} = \Phi_{surf} + \Phi_{wake} + \Phi_{vortex} - P_{K_{in}} \quad (7)$$

It has been shown that in the case where the propulsors are located at the trailing edge of the fuselage, the surface dissipation on the airframe is only weakly affected by engine operating condition, and thus the assumption can be made that the surface dissipation for the integrated vehicle is the same as that for the isolated airframe.⁶ Additionally, one can also make the assumption that the propulsor does not affect the dissipation of trailing vortex system far downstream. Thus, Eq. (7) can be written as:

$$P_{K_{out}} - \Phi_{jet} = \Phi'_{surf} + \Phi'_{vortex} + \Phi'_{wake} - (\Delta\Phi_{wake} + P_{K_{in}}) \quad (8)$$

where (') terms denote expressions calculated for the non-BLI configuration. $\Delta\Phi_{wake}$ represents the reduction in wake dissipation between the non-BLI and a BLI configuration. Based on the definitions for P_K and Φ_{jet} , for a simple 1-D analysis it can be shown that the left hand side of Eq. (8) reduces to:

$$P_{K_{out}} - \Phi_{jet} = [\dot{m}_{out} (V_j - V_\infty) + (p_e - p_\infty) A_e] V_\infty \quad (9)$$

This expression is equivalent to the freestream ram drag subtracted from the nozzle gross thrust, and for a podded engine is equal to the net thrust times flight velocity. For the non BLI case, given $\Delta\Phi_{wake}$ and $P_{K_{in}}$ are zero, Eq. (8) reduces to:

$$\underbrace{P'_{K_{out}} - \Phi'_{jet}}_{F_N V_\infty} = \underbrace{\Phi'_{surf} + \Phi'_{vortex} + \Phi'_{wake}}_{D' V_\infty = \Phi'_{tot}} \quad (10)$$

The propulsion system is sized for a fixed difference of $P_{K_{out}}$ and Φ_{jet} . Thus, one can see that the benefit of BLI comes from reduction in jet and wake dissipation. For a BLI configuration, Eq. (8) is the main modeling challenge. Changes in the propulsor design or operating condition will cause changes in the upstream flow field and ingested boundary layer, and thus there is a coupling between the propulsion system and airframe aerodynamics. Solving an MDA problem using a fully coupled Propulsion-RANS model as shown in work by Gray⁸ can be extremely useful for analyzing a given system. However, for the conceptual design of a BLI propulsion system, a stage that involves design space exploration studies, it is preferable to minimize the amount of CFD required, while still capturing the physics unique to BLI systems as efficiently as possible to avoid erroneous performance predictions. This leads to a natural question - how can a BLI propulsion system be designed in the conceptual phase that efficiently takes into account the effect of propulsion on aerodynamics and vice versa? Current literature shows a gap in the required fidelity and accuracy of modeling BLI propulsion systems in the conceptual design phase. This paper tries to fill the gap and in the process also attempts to quantify the sensitivity of the ingested boundary layer to the propulsion system design.

In this paper, nacelle diameter and throttle setting are the on-design and off-design propulsion system parameters respectively that are assumed to create any upstream flow field changes. Capturing the variation in $\Delta\Phi_{wake}$ and $P_{K_{in}}$ as a function of these parameters can help quantify the interdependency between aerodynamics and propulsion. The change in the ingested flow distribution also changes the flow distortion into the fan, which leads to differences in fan and nozzle losses.

C. BLI Impacts on Losses in the Propulsor

Distortion is inherent in boundary layer flow and this can negatively impact the performance of a BLI engine. BLI modeling remains incomplete if losses due to distortion are not taken into account. Distortion (especially, total pressure distortion) causes a drop in fan efficiency and if not attenuated, also results in nozzle losses. Several authors have tried to include loss models while performing propulsion system analysis and design for BLI engines. Liu⁹ conducted cycle analysis on the TeDP concept with BLI, accounting for inlet recovery losses. Nozzle and fan losses due to BLI were not captured. Felder¹⁰ also studied the effect of BLI on TeDP and included fan losses using a trend curve for efficiency drop, but kept the nozzle coefficients fixed. Shi¹¹ conducted the system assessment of BLI engines with different fidelities of loss models to highlight that losses in the inlet, fan, and nozzle all need to be captured to properly analyze the trade-offs and realize the true benefit of a BLI system. However, this study did not analyze the impact of propulsion system parameter changes on the ingested flow field.

To realistically model the performance of a BLI propulsion system, this paper will use the environment in GT-HEAT developed by Shi that incorporates a modified parallel compressor model¹² and nozzle model¹³ in the framework setup by Gladin.¹⁴ CFD is used to isolate the effects of the propulsors on the flow field and consequently, the boundary layer that the propulsor ingests. First, the difference between the uncoupled (where the throttle dependent effects on flow field are not captured) and coupled models are assessed. Second, the flow properties of interest to the propulsion system are modeled as functions of propulsion system parameters. All analyses are performed on a fixed airframe. The remainder of this paper is organized as follows: The methodology for modeling the boundary layer through CFD and the propulsion system using GT-HEAT will be discussed in section III. Next, the results will be discussed in section IV. Finally, the conclusions and potential future work will be discussed in section V.

III. Modeling Methodology

This section describes the modeling methodology for developing the propulsion system and aerodynamic models. In the coupled aerodynamics-propulsion problem, both models require information from each other, and this information is passed in the form of coupling variables. One can either directly integrate CFD and the engine cycle model in an MDA solver, as has been done in literature, or to minimize the computational burden of running several MDA problems for each propulsor design case, generate a surrogate of the CFD responses as a function of the propulsion variables. These aerodynamic surrogates can then be used with the cycle model in the MDA solver setup. Details of the model and the information being passed are discussed in the following sections.

A. BLI Propulsion Model

The propulsion model is a 1-D thermodynamic model using performance maps. Details of the overall application in BLI propulsion systems can be found in Refs.^{11,15} In addition, the inlet model is modified to include the effect of ingesting boundary layer flow. Combining Eqns.(8) - (10) in a 1-D formulation for cruise, one gets:

$$[\dot{m}_{out} (V_j - V_{\infty} = \infty) + (p_e - p_{\infty}) A_e] V_{\infty} = D'V_{\infty} - (\Delta\Phi_{wake} + P_{K_{in}}) \quad (11)$$

The left hand side of Eq. (11) can be computed from the propulsion model, while the requirement for the propulsion model, i.e. the right hand side, is computed from CFD. Fig. 1 shows the architecture of the propulsion model used for this study. The propulsor is a distributed ducted fan that is driven by an electric transmission, which in turn is powered by a gas generator.

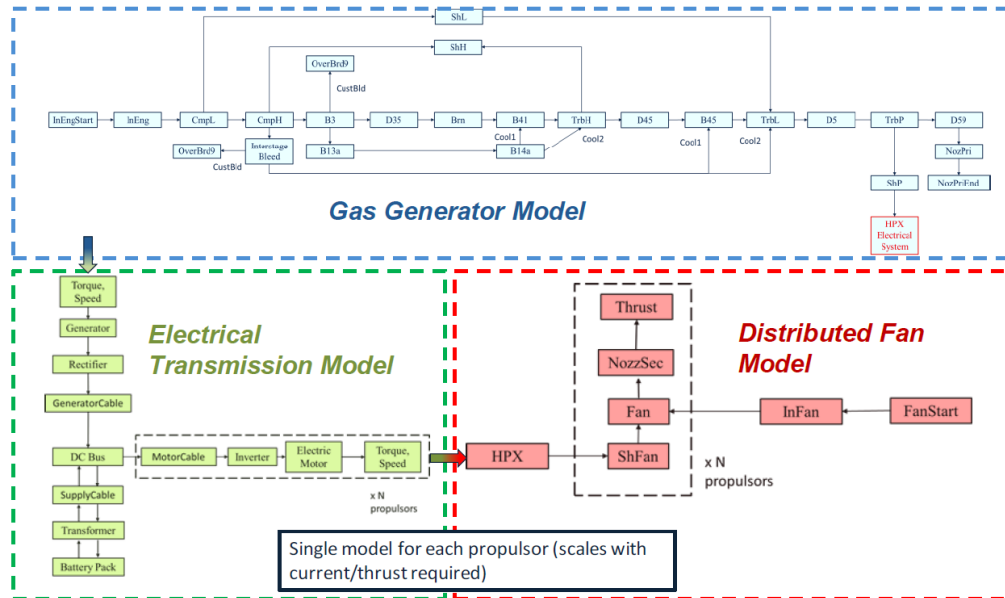


Figure 1. Architecture of the propulsion model

1. Distortion Impacts: Fan

Although no distortion terms appear in Eq. (11), the presence of distortion indirectly affects the outputs of the propulsion system and manifests as component losses. In order to assess the impacts of distortion on fan performance, a modified Parallel Compressor (PC) model developed by Pokhrel¹² is used in this study. The conventional PC model treats the incoming flow as two parallel streams: one distorted and the other clean with uniform properties at each stream and assumes constant static pressure at the fan exit of both sectors. In contrast to the conventional approach, the modified PC model corrects the static pressure boundary condition by taking into account the strength of distortion as shown in Eq. (12).

$$p_{\text{clean}} = \left(1 + \frac{dPcP_{\text{crit}}}{2} \right) p_{\text{dist}} \quad (12)$$

Here, p_{clean} and p_{dist} refer to the static pressures at the exit of the clean and distorted sectors respectively. $dPcP_{\text{crit}}$ is the intensity of distortion at critical angle value.¹² The implemented architecture of the parallel compressor model is shown in Fig. 2.

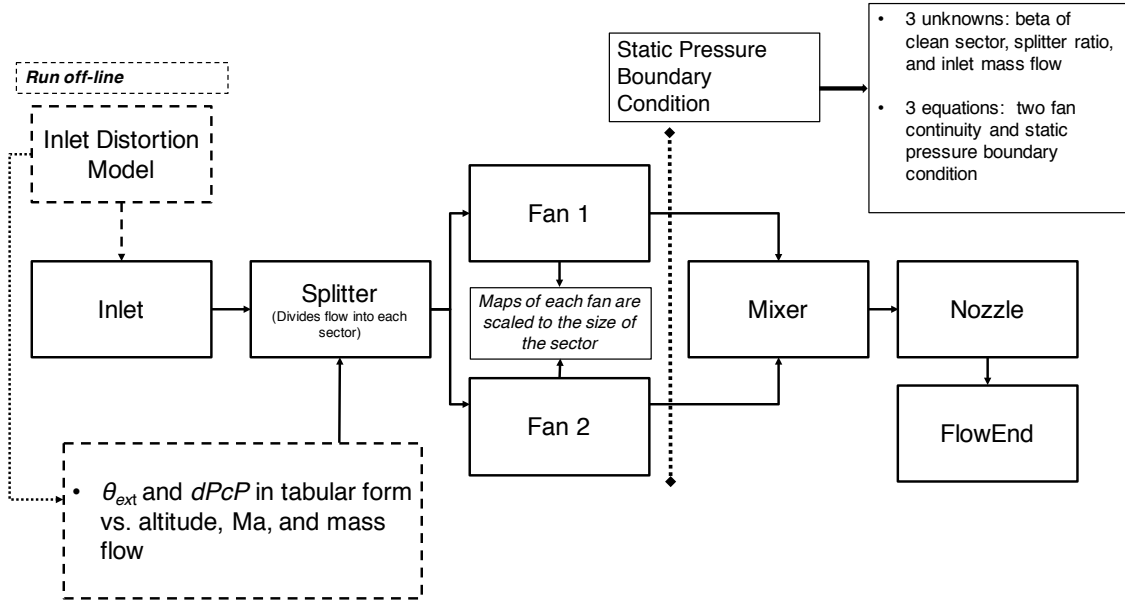


Figure 2. Parallel compressor model architecture

2. Distortion Impacts: Nozzle

The nozzle model built by Shi¹³ is used to analyze the impacts of distortion on the discharge coefficient and gross thrust coefficient. The loss model is a combination of an analytic turbulent pipe flow solution and a mixing model that predicts the pressure drop using the generated entropy through the nozzle, as shown in Fig. 3. Based on the architecture of the model, some additional inputs are required for the inflow condition that defines the distortion. The required flow inputs are shown in Table 1.

B. BLI Aerodynamic Model and Geometry

Ideally, one would like to perform CFD analysis on the complete airframe to get the Φ' terms in Eq. (8). At the conceptual design stage however, the airframe OML is fluid and thus CFD is usually not employed at this stage to obtain estimates for drag (Φ'/V_∞). A drag buildup approach based on wetted areas can be used to obtain initial estimates for the vehicle. To simplify the analysis in this study, CFD is only used to capture quantities that change, going from the non-BLI to the BLI case, as described before.

To further reduce the computational expense, instead of using a full 3-D fuselage with partially embedded engines, an axisymmetric fuselage with an aft mounted fan is used as the geometry for obtaining reasonable estimates of the boundary layer related terms for the full 3-D case. The dimensions of the geometry are

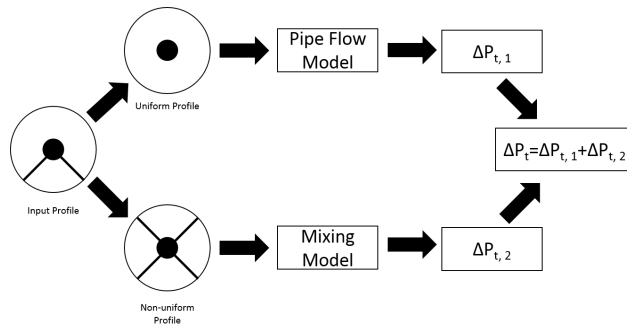


Figure 3. Nozzle pressure drop calculation process¹³

Table 1. Distortion information inputs to the propulsion model

Parameter	Notation	Description
Intensity	$dPcP$	Distortion intensity ($dPcP = 1 - \frac{p_{t_{low}}}{p_{t_{avg}}}$)
Extent	θ	Circumferential extent of the distorted sector
Low Pressure	$p_{t_{low}}$	Average total pressure of low pressure region
High Pressure	$p_{t_{high}}$	Average total pressure of high pressure region
Average Pressure	$p_{t_{avg}}$	Average total pressure

similar to a 737-8 fuselage, as seen in the cross section view in Fig. 4. Compared to a full 3-D geometry, the CFD run time for an axisymmetric model is an order of magnitude lower. Though the geometry modeled in CFD is axisymmetric, the actual distortion analysis and propulsor sizing is done for a partially embedded nacelle in the fuselage case. To this effect, the fan height in the axisymmetric model is thus the nacelle diameter for the transformed case.

In this analysis, the fuselage shape is fixed and only propulsion parameters are varied. The baseline case is a clean fuselage (nacelle absent). For a nominal steady level flight condition (35,000 ft and Mach 0.85), twenty-five cases (Table 2) are run for a range of fan diameters and static pressures at the fan face (flow station 2). The fan face is modeled as a pressure outlet in CFD, where uniform static pressure and temperature values are imposed, while the fan exit is modeled as a stagnation inlet, with uniform total pressure and temperature boundary conditions. A nominal pressure ratio is prescribed at the fan face to impose the downstream boundary conditions. Table 3 lists the flow property distributions captured from the CFD analyses.

Table 2. Parameters of interest for Design of Experiments

Parameter	Lower Bound Value	Upper Bound Value	Number of Levels
Fan Diameter (d2)	26.7 in	42.0 in	5
Fan Face Static Pressure (P2)	19 kPa	27 kPa	5

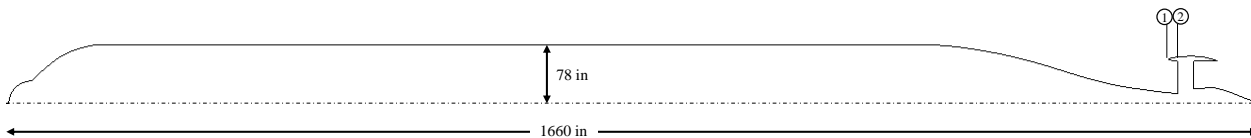


Figure 4. Notional geometry of interest

Table 3. Responses of interest from CFD

Distribution	Notation	Location
Total Pressure	p_{t_1}	Inlet Highlight
Static Pressure	p_1	Inlet Highlight
Velocity	V_1	Inlet Highlight
Density	ρ_1	Inlet Highlight
Mass flux	m_{flux}	Inlet Highlight
Total Pressure	p_{t_2}	Fan Face

To model the transformed geometry (partially embedded engines in a fuselage), all field distributions in Table 3 are extruded such that the boundary layer properties are symmetrical about the vertical diameter. For these updated distributions, one can now compute $P_{K_{in}}$ and $\Delta\Phi_{\text{wake}}$ as follows:⁶

$$P_{K_{in}} = \iint - \left[(p_1 - p_\infty) + \frac{1}{2} \rho (V_1^2 - V_\infty^2) \right] \mathbf{V}_1 \cdot \hat{\mathbf{n}} dA_1 \quad (13)$$

$$\Delta\Phi_{\text{wake}} = \Phi'_{\text{wake}} - \Phi_{\text{wake}} = \frac{\kappa_{in}}{\Phi'_{\text{surf}}} \Phi'_{\text{wake}} \quad (14)$$

In Eq. (13), A_1 is the inlet area at flow station 1, as shown in Fig. 4. In Eq. (14), $\Delta\Phi_{\text{wake}} > 0$ for the BLI case where a portion of the wake is ingested by the engine. The surface dissipation (Φ'_{surf}) and ingested kinetic energy defect (κ_{in}) are calculated using Eq. (15) at the trailing edge of the clean fuselage and the propulsor inlet for the integrated cases respectively.

$$\kappa(x) = \iint \frac{1}{2} (V_{ed}^2 - V^2) \rho V dS(x) \quad (15)$$

Lastly, the wake dissipation for the non-BLI case is obtained using Eq. (16) evaluated at the trailing edge of the clean fuselage as follows:

$$\Phi'_{\text{wake}} = \iint \frac{1}{2} (V_{ed} - V)^2 \rho V dS(x = x_{TE}) \quad (16)$$

For the loss models discussed above, distortion information at the fan face needs to be provided. All parameters mentioned in Table 1 are computed for each case in the DoE, with mass flow averaging used to obtain averaged quantities where required.

C. MDA Problem Formulation

Table 4 shows the aero-propulsive coupling problem that needs to be solved. The MDA architecture is illustrated in Fig. 5. For a given flight condition and an airframe, $\Phi'_{\text{tot}} = \Phi'_{\text{surf}} + \Phi'_{\text{wake}} + \Phi'_{\text{vortex}}$ is computed. Φ'_{surf} and Φ'_{wake} are computed from Eq. (15) and (16) respectively. The remaining component, Φ'_{vortex} , is the dissipation in the trailing vortex sheet and is proportional to the induced drag, D'_i . For the purposes of this study, since the entire airframe is not considered, the vortex dissipation is assumed to be approximately 10% of the total dissipation. The Φ' terms on the right side of Eq. (8) are now known. $P_{K_{in}}$ and $\Delta\Phi_{\text{wake}}$ come from the surrogate models of the aerodynamic analysis. Compatibility between the aerodynamics and propulsion disciplines is achieved by driving the three residual equations shown in Table 4 to zero. The propulsor is sized (in on-design mode) or throttled (in off-design analysis) to match the 1-D power balance equation. The blockage factor, which corrects the uniform flow assumption made by propulsion model by accounting for the mass defect in the ingested boundary layer, and the pressure recovery guess in the propulsion model are also perturbed to achieve interdisciplinary compatibility.

Table 4. MDA Problem Formulation

Residuals	Solver Variables
$R_1 = [\dot{m}_{NPSS} (V_j - V_\infty) + (p_e - p_\infty) A_e] V_\infty - D'V_\infty + (\Delta\Phi_{wake} + P_{K_{in}})$	Fuel flow (\dot{m}_f)
$R_2 = \dot{m}_{CFD} - \dot{m}_{NPSS}$	Blockage factor (λ)
$R_3 = \eta_{PR_{CFD}} - \eta_{PR_{NPSS}}$	Pressure recovery ($\eta_{PR_{NPSS}}$)

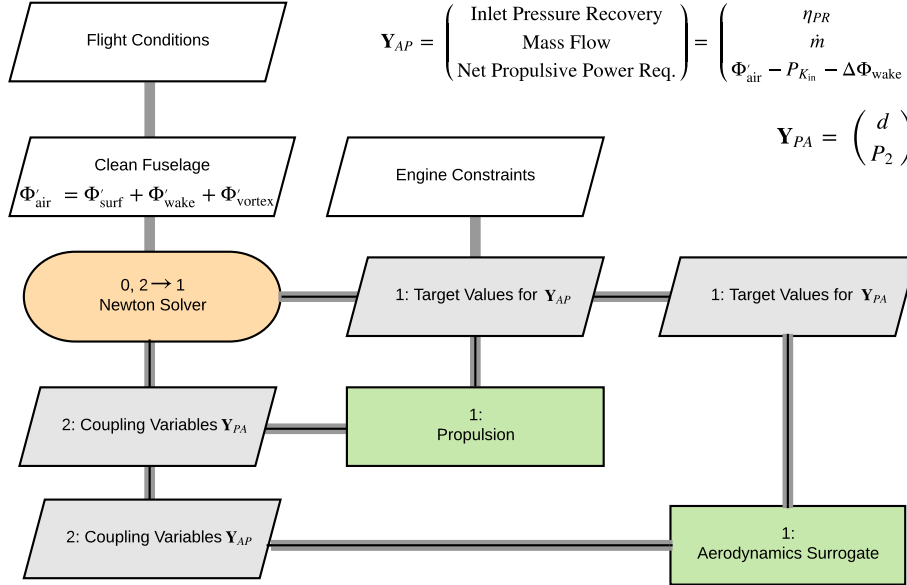


Figure 5. XDSM diagram showing the aero-propulsive coupling problem

D. Integration Environment

The analysis presented in this paper is done through a combination of two platforms: CFD modeling is done through the commercially available STAR-CCM+ and the propulsion system is modeled through Georgia Tech Hybrid Electric Analysis Tool (GT-HEAT).^{16–18} GT-HEAT is an environment for aircraft sizing and synthesis, which was developed by Georgia Tech. In this environment, vehicle mission analysis is represented by an engine assembly, an airframe assembly (vehicle analysis module), and a mission assembly. Each assembly is a self-contained analysis module which contains multiple sub-analyses modules.

IV. Results

Results of the modeling methodology outlined in section III are presented. The uncoupled case here refers to the design and analysis of the propulsor where the impact of flow properties on the propulsion system is considered but the throttle dependent impacts on the flow field is not considered. Flow properties for the uncoupled case are obtained from CFD using a through flow nacelle instead of a powered engine. The coupled case implies solving the MDA problem shown in Fig. 5, and includes the effect of the propulsor on the flow field. The surrogate models of the flow properties of interest are modeled as a function of propulsor design (diameter) and the operating condition (fan face static pressure) as outlined before. Thermodynamic property profiles at the trailing edge of a clean fuselage (nacelle absent) are also extracted to obtain estimates for Φ'_{wake} and Φ'_{surf} , used in the computation of $\Delta\Phi_{wake}$. Trends in the flow properties obtained from CFD are shown first, followed by an analysis into the differences in propulsor performance and sizing between the coupled and uncoupled cases.

A. CFD Results

Fig. 6 compares the axial velocity, total and static pressure, and density profiles at the inlet highlight plane, along with the total pressure profile at the fan face, for two different p_2 values at a fixed fan diameter. The y axis represents normalized height from the fuselage surface to the inlet lip. The fan face static pressure boundary condition can be mapped to the throttle setting of the engine. A higher p_2 , corresponding to the engine operating at a lower throttle, slows the incoming flow relative to a lower p_2 (higher throttle), which increases the suction and thus increases incoming flow velocity. This can be seen in the axial velocity comparison plot in Fig. 6. While the static pressure of the flow at inlet highlight also increases due to the increase in p_2 , the total pressure drops. p_{t1} and p_{t2} are influenced strongly by the change in velocity, which is indicative of higher losses in the flow at increased p_2 .

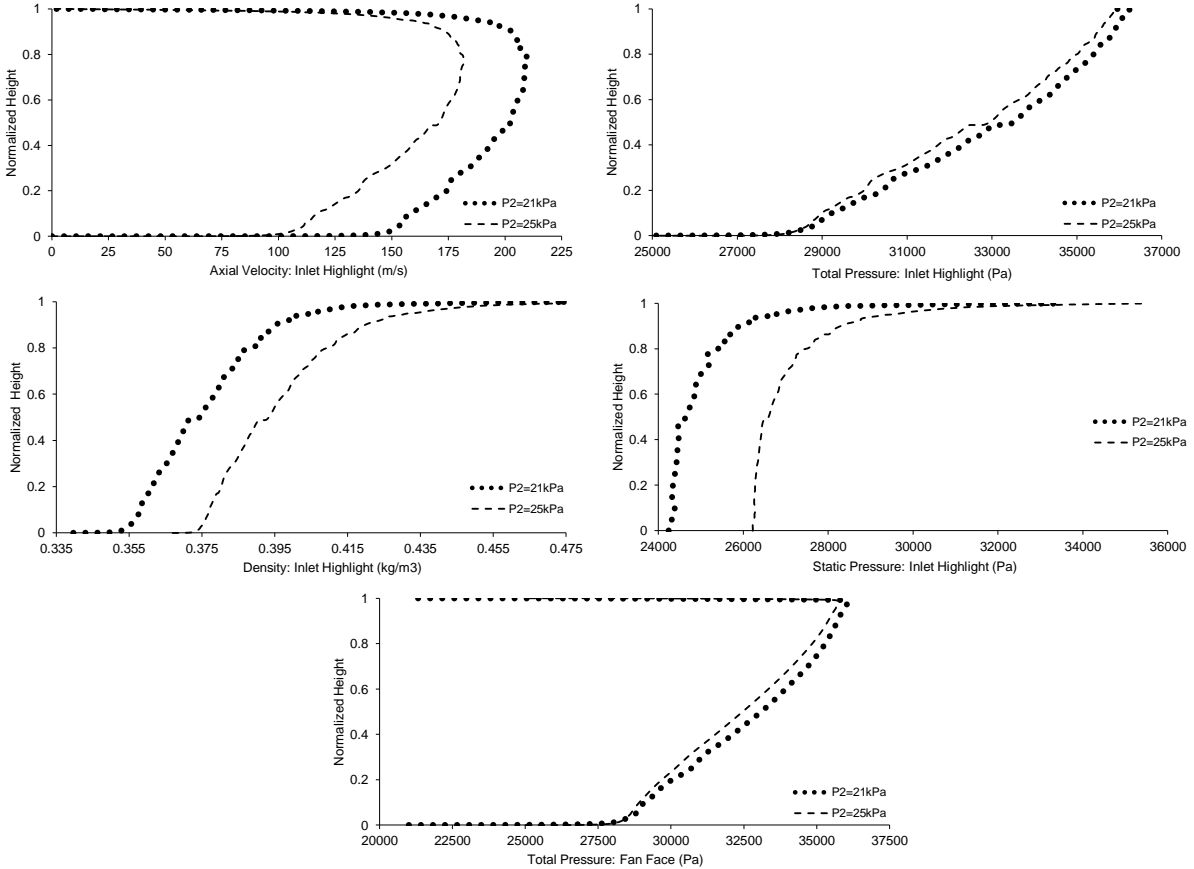


Figure 6. Boundary Layer Flow Properties ($d_2 = 92$ in. $p_2 = 21$ and 25 kPa)

For all the DoE cases, $P_{K_{in}}$ and $\Delta\Phi_{wake}$ are calculated using Eqns. (13) and (14). In addition, all distortion parameters from Table 1 are also computed. In the figures that follow, the fan diameter and static pressure at the fan face are normalized using Eqns. (17) and (18) where d_1 is the smallest diameter and d_h is the largest diameter fan considered in the DoE.

$$d^* = \frac{d - d_1}{d_h - d_1} \quad (17)$$

$$p_2^* = \frac{p_2}{p_\infty} \quad (18)$$

Fig. 7 shows the variation of $P_{K_{in}}$ with respect to the fan diameter and the fan face static pressure. The ordinate is $P_{K_{in}}$ normalized by $P_{K_{in-base}}$, where $P_{K_{in-base}}$ is the value of flow power going into a hypothetical propulsor large enough to capture the entire boundary layer. Therefore, the y axis represents the fraction of the mechanical power in the boundary layer that is captured by the propulsor. An increase in fan

diameter results in an increase in $P_{K_{in}}$. This is a direct consequence of ingesting a larger percentage of the boundary layer flow. The variation with fan diameter is roughly linear. As the throttle setting is increased (p_2 decreases), $P_{K_{in}}$ increases for a given diameter. For a unit normal vector at the inlet highlight plane, pointing inwards towards the fan face, and parallel to the incoming velocity, $P_{K_{in}}$ can be expressed as

$$P_{K_{in}} = \iint \left[(p_\infty - p_1) + \frac{1}{2}\rho(V_\infty^2 - V_1^2) \right] V_1 dA_1 \quad (19)$$

As seen in Fig. 6, decreasing p_2 increases V_1 and decreases p_1 . Thus, $(p_\infty - p_1)$ increases as p_2 decreases, but $(V_\infty^2 - V_1^2)$ decreases. Since $V_1 < V_\infty$, $(V_\infty^2 - V_1^2) > 0$. Additionally, since these terms are multiplied by V_1 , the net effect is an increase in $P_{K_{in}}$. However, compared to the impact of the propulsor size, the throttle setting is a less significant factor.

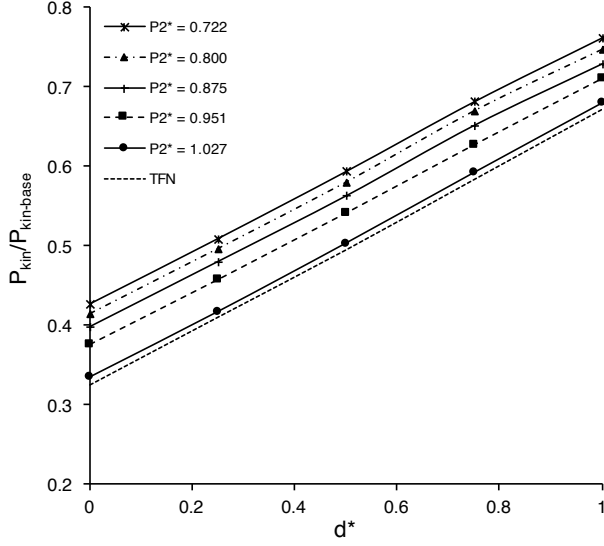


Figure 7. Variation of $P_{K_{in}}$

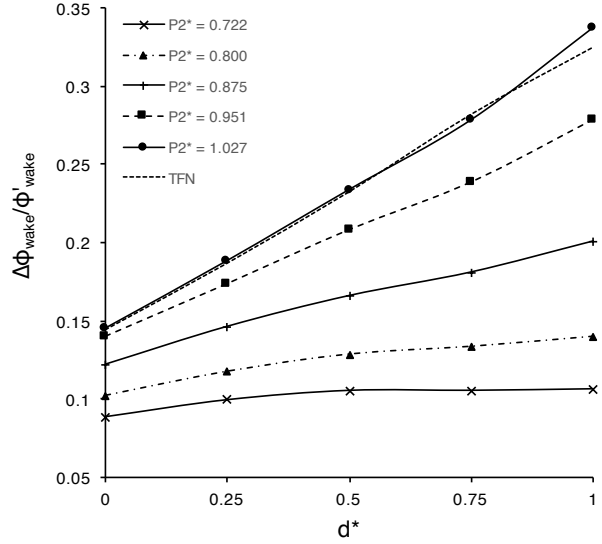


Figure 8. Variation of $\Delta\Phi_{wake}$

Figure 8 shows the variation of $\Delta\Phi_{wake}$ normalized by the wake dissipation on a clean fuselage (Φ'_{wake}). With an increase in propulsor size, a higher reduction in wake dissipation is observed compared to the clean fuselage. In an ideal case, if the propulsor was large enough to ingest the entire boundary layer, then $\Delta\Phi_{wake}$ would equal to Φ'_{wake} . This means that there would be no wake dissipation contribution from the fuselage. Unlike what is observed for $P_{K_{in}}$, Φ'_{wake} does not have a linear trend with d_2 . It's nonlinear with p_2 as well. This is because the local edge velocity changes with d_2 and p_2 . If the edge velocity was insensitive to pressure and diameter, then the trends would be more linear with d_2 . An increase in p_2 reduces the velocity, which increases the kinetic energy defect in the ingested boundary layer flow. A higher defect in the ingested flow corresponds to a higher $\Delta\Phi_{wake}$ as evident from Eq. (14).

The magnitude of $\Delta\Phi_{wake}$ is relatively small compared to $P_{K_{in}}$. The ratio of $\Delta\Phi_{wake}$ to $P_{K_{in}}$ as a function of p_2 and d_2 is shown in Fig. 9. For a given p_2 , the ratio of $\Delta\Phi_{wake}$ to $P_{K_{in}}$ remains approximately constant for all diameters, while for a given diameter, this ratio increases with an increase in p_2 . From the definitions of $P_{K_{in}}$ in Eq. (19) and $\Delta\Phi_{wake}$ in Eq. (14), we see that the ratio of the two values is proportional to the change in pressure and velocity at the inlet highlight as follows:

$$\frac{\Delta\Phi_{wake}}{P_{K_{in}}} \propto \frac{V_{ed}^2 - V_1^2}{(V_\infty^2 - V_1^2) + (p_\infty - p_1)} \quad (20)$$

As the fan diameter is increased for a given p_2 , there is a more noticeable impact on the ΔV terms than there is on the Δp term. As a result, the ratio of $\Delta\Phi_{wake}$ to $P_{K_{in}}$ is roughly constant with diameter. However, as p_2 is increased, Δp decreases, and as a result, for a given diameter the ratio of $\Delta\Phi_{wake}$ to $P_{K_{in}}$ increases.

Pressure recovery variation with d_2 and p_2 can be observed in Fig. 10. The mass averaged total pressure in larger propulsor is higher as it ingests a larger percentage of flow closer to freestream conditions. As a result, pressure recovery increases with increasing fan diameter. An increase in p_2 results in a more adverse

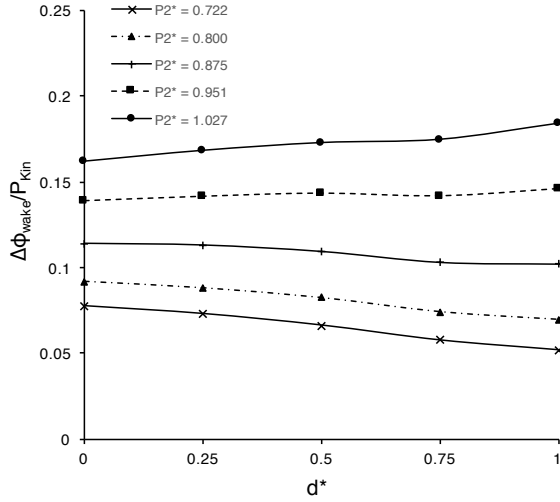


Figure 9. Relative contribution of $\Delta\Phi_{wake}$ and P_{Kin}

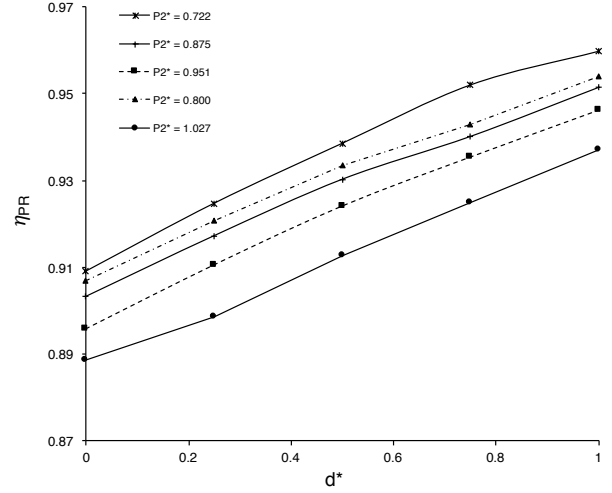


Figure 10. Variation of η_{PR}

pressure gradient, which results in a larger total pressure loss in the flow, and thus a smaller pressure recovery.

Generating the Surrogate Models

The 25 data points are used to fit a first order linear regression model for the variation of P_{Kin} with respect to d_2 and p_2 . This is by no means a generalized equation as it only applies to the fuselage used, for the ranges of fan diameters and fan face static pressures applied. R^2 for the training and validation data is 0.99. For $\Delta\Phi_{wake}$, since the trends are non-linear due to the variation in edge velocity, a second order linear regression model is used to capture this variation with R^2 of 0.98 for both training and validation data. Similarly, second order linear regression models for mass flow and pressure recovery with satisfactory statistical measures are created. Distortion parameters are generated as simple lookup tables for use in the propulsion model.

B. Propulsor Performance Difference: Coupled vs. Uncoupled

The results shown here quantify the difference in propulsor performance between the coupled and uncoupled analyses. BLI benefits can be assessed in multiple ways. In this study, two fixed propulsors are analyzed. Both are sized at different diameters to produce the same thrust on a non-BLI configuration. Both coupled and uncoupled analysis models are used to predict fuel burn and BLI effect [Eq. (21)]. Table 5 shows the percentage difference in the predicted results between the uncoupled (u) and the coupled (c) analyses.

$$\text{BLI Effect} \equiv \zeta = P_{Kin} + \Delta\Phi_{wake} \quad (21)$$

Table 5. Performance Difference: Uncoupled - Coupled

Case	d2 (in.)	$\% \Delta \dot{m}_f$	$\% \Delta \zeta$
1	26.7	4.80%	-5.23%
2	32.0	3.64%	-3.82%

$$\% \Delta \dot{m}_f = \frac{\dot{m}_{f_u} - \dot{m}_{f_c}}{\dot{m}_{f_c}} \times 100 \quad (22)$$

$$\% \Delta \zeta = \frac{\zeta_u - \zeta_c}{\zeta_c} \times 100 \quad (23)$$

For both cases, the uncoupled analysis predicts a lower BLI effect, and thus a higher fuel burn than the coupled analysis. The percent difference in the BLI effect is larger at smaller diameters. Consequently, there is a larger difference in fuel burn between the coupled and uncoupled analyses for smaller propulsors. What this implies, is for a very large propulsor, the difference between uncoupled and coupled analysis may be negligible because the sensitivity of the BLI effect on the throttle condition decreases with increase in diameter. However, for configurations with smaller propulsors, the coupling needs to be considered and an iterative procedure has to be implemented.

C. Propulsor Design Difference: Coupled vs. Uncoupled

The proposed approach can also be applied to size a propulsor. In this study, the propulsor is sized only at a single design point (cruise). The goal is to design a propulsor for a BLI configuration, and two propulsors are designed - one using a coupled approach and another using uncoupled. For both cases, the propulsor was sized to produce the same net momentum flux as given by Eq. (24). It is observed that the uncoupled approach predicts a higher fan diameter and fuel burn by 2.02% and 3.38% respectively compared to the coupled case, which stems from the 1.5% lower BLI effect prediction from the uncoupled analysis.

$$P_{K_{out}} - \Phi_{jet} + (\Delta\Phi_{wake} + P_{K_{in}}) = D'V_{\infty} \quad (24)$$

V. Summary and Future Work

The present work demonstrated a novel approach for performing a coupled aero-propulsive analysis with the consideration of distortion impacts on the fan and nozzle. Rather than integrating CFD directly with the cycle model in an MDA solver, which is computationally expensive if several propulsor designs are being considered, the aero-propulsive coupling problem was handled by generating surrogates and look up tables of the aerodynamics model, and then iterating using these computationally cheaper analyses. The power balance approach developed by Drela was used instead of the conventional momentum approach to avoid any confusion with thrust and drag bookkeeping. Interdisciplinary compatibility was achieved through a Newton solver in NPSS, which perturbed the engine throttle setting, blockage factor, and pressure recovery to drive the residual equations defining the MDA problem to zero.

For the cases investigated, the results showed that an uncoupled analysis underestimates the fuel burn benefit from BLI, and the difference is generally observed to be higher for a smaller propulsor. In this study, the comparison between a non BLI and BLI configuration is not made given that a complete airframe is not modeled. Thus, it does not make sense to demonstrate the BLI benefit relative to a podded configuration. While the current study only considered a single flight condition, it would be interesting to analyze the BLI benefit for the entire mission considering a coupled approach for a complete airframe. Further scaling laws on the boundary layer profile based on different flight conditions should be employed. A multi-design point approach for sizing the engines should also be considered.

References

- ¹Suder, K., “Overview of the NASA Environmentally Responsible Aviation Project’s Propulsion Technology Portfolio,” *48th AIAA-ASME-SAE-ASEE Joint Propulsion Conference and Exhibit, Joint Propulsion Conferences*, 2012.
- ²Smith, A., “The jet airplane utilizing boundary layer air for propulsion,” *Journal of the Aeronautical Sciences*, Vol. 14, No. 2, 1947, pp. 97–109.
- ³Gearhart, W. S. and Henderson, R. E., “Selection of a Propulsor for a Submersible System,” *Journal of Aircraft*, Vol. 3, No. 1, 1966, pp. 84–90.
- ⁴Wislicenus, G. F., “Hydrodynamics and propulsion of submerged bodies,” *ARS Journal*, Vol. 30, No. 12, 1960, pp. 1140–1148.
- ⁵Liu, Y., Elham, A., Horst, P., and Hepperle, M., “Exploring Vehicle Level Benefits of Revolutionary Technology Progress via Aircraft Design and Optimization,” *Energies*, Vol. 11, No. 1, 2018, pp. 166.
- ⁶Hall, D. K., Huang, A. C., Uranga, A., Greitzer, E. M., Drela, M., and Sato, S., “Boundary Layer Ingestion Propulsion Benefit for Transport Aircraft,” *Journal of Propulsion and Power*, 2017, pp. 1–12.
- ⁷Drela, M., “Power Balance in Aerodynamic Flows,” *AIAA Journal*, Vol. 47, No. 7, 2009.
- ⁸Gray, J. and Martins, J. R., “Approach to Modeling Boundary Layer Ingestion using a Fully Coupled Propulsion-RANS Model,” 2017.
- ⁹Liu, C., Dougeris, G., Laskaridis, P., and Singh, R., “Thermal cycle analysis of turboelectric distributed propulsion system with boundary layer ingestion,” *Aerospace Science and Technology*, Vol. 27, No. 1, 2013, pp. 163–170.
- ¹⁰Felder, J., Kim, H., Brown, G., and Kummer, J., “An examination of the effect of boundary layer ingestion on turboelectric distributed propulsion systems,” *49th AIAA aerospace sciences meeting including the new horizons forum and aerospace exposition*, 2011, p. 300.
- ¹¹Shi, M., Pokhrel, M., Gladin, J. C., Garcia, E., and Mavris, D. N., “Model Fidelity Requirements in Boundary Layer Ingestion Propulsion System Conceptual Design,” *18th AIAA Aviation Technology, Integration, and Operations Conference, AIAA AVIATION Forum (AIAA 2018-3835)*, 2018, doi: 10.2514/6.2018-3835.
- ¹²Pokhrel, M., Gladin, J. C., Garcia, E., and Mavris, D. N., “A Methodology for Quantifying Distortion Impacts Using A Modified Paralell Compressor Theory,” *To be published in the ASME Turbo Expo 2018, Lillestrom(Oslo), Norway*, 2018.
- ¹³Shi, M., Pokhrel, M., Gladin, J. C., Garcia, E., and Mavris, D. N., “Convergent Nozzle Gross Thrust Coefficient and Discharge Coefficient Calculation with Boundary Layer Ingestion (BLI) Effects,” *53rd AIAA/SAE/ASEE Joint Propulsion Conference, (AIAA 2017-5057)*, 2017, doi: 10.2514/6.2017-5057.
- ¹⁴Gladin, J. C., *A sizing and vehicle matching methodology for boundary layer ingesting propulsion systems*, Ph.D. thesis, Georgia Institute of Technology, 2015.
- ¹⁵Shi, M., Pokhrel, M., Gladin, J. C., Garcia, E., and Mavris, D. N., “Modeling Fidelity Requirements of Mission-Level Analysis on Boundary Layer Ingestion Propulsion System,” *2019 AIAA Aerospace Sciences Meeting, AIAA SciTech Forum*, 2019.
- ¹⁶Perullo, C., Tai, J., and Mavris, D., “A New Sizing and Synthesis Environment for the Design and Assessment of Advanced Hybrid and Electric Aircraft Propulsion Systems,” *International Association of Airbreathing Engines (ISABE)*, 2015.
- ¹⁷Gladin, J. C., Perullo, C., Tai, J. C., and Mavris, D. N., “A Parametric Study of Hybrid Electric Gas Turbine Propulsion as a Function of Aircraft Size Class and Technology Level,” *55th AIAA Aerospace Sciences Meeting*, 2017, p. 0338.
- ¹⁸Gladin, J., Trawick, D., Perullo, C., Tai, J. C., and Mavris, D. N., “Modeling and Design of a Partially Electric Distributed Aircraft Propulsion System with GT-HEAT,” *55th AIAA Aerospace Sciences Meeting*, 2017, p. 1924.